Evidence for pseudo–Jahn-Teller distortions in the charge density wave phase of $1T$-$TiSe_2$

A. Wegner,[1] J. Zhao,[1] J. Li,[1] J. Yang,[2] A. A. Anikin,[3] G. Karapetrov,[3] K. Esfarjani,[4,1,5] D. Louca,[1,*] and U. Chatterjee[1,†]

[1]*Department of Physics, University of Virginia, Charlottesville, Virginia 22904, USA*
[2]*Department of Physics, Central Michigan University, Mount Pleasant, Michigan 48859 22904, USA*
[3]*Department of Physics, Drexel University, 3141 Chestnut Street, Philadelphia, Pennsylvania 19104, USA*
[4]*Department of Mechanical and Aerospace Engineering, University of Virginia, Charlottesville, Virginia 22904, USA*
[5]*Department of Materials Science and Engineering, University of Virginia, Charlottesville, Virginia 22904, USA*

(Received 11 June 2018; revised manuscript received 5 April 2020; accepted 23 April 2020; published 27 May 2020)

The charge density wave (CDW) instability in $1T$-$TiSe_2$ is revisited to investigate its electronic and structural origins using angle resolved photoemission spectroscopy (ARPES), neutron diffraction, and density functional theory (DFT) calculations. The evidence for Jahn-Teller (JT)-like distortions in the CDW state is provided from the local structure analysis that shows splitting of the Ti-Se bonds into short and long. The magnitude of the split is inconsistent with the commonly accepted Di Salvo model for the structural distortions in the CDW phase. From the APRES data, it is deduced that a nontrivial temperature-dependent energy shift of the Se $4p$ valence bands occurs, but is absent for the Ti $3d$ conduction bands. Collectively, these observations suggest that a JT-like mechanism is most likely central to the CDW instability in $1T$-$TiSe_2$.

DOI: 10.1103/PhysRevB.101.195145

I. INTRODUCTION

In strongly correlated systems, emergent properties often lead to competition or coexistence of proximate broken symmetry phases. The cuprate [1] and pnictide [2] high temperature superconductors, colossal magnetoresistive manganites [3], and heavy fermion compounds [4] are examples in which the presence of multiple degrees of freedom can give rise to exotic phenomena. Understanding of the phase competition/coexistence in these strongly correlated systems is, however, intractable due to their intricate electronic and crystal structures. $1T$-$TiSe_2$, a transition metal dichalcogenide [5,6] CDW compound is a model system through which the interplay of multiple degrees of freedom can be studied. This is due to the prototypical nature of its CDW order, and its relatively simple crystalline and electronic structures. $1T$-$TiSe_2$ becomes superconducting in a field-effect transistor configuration [7], via chemical intercalation [8] or pressure [9], and has the characteristic dome shape that resembles those of high temperature superconductors and heavy fermion compounds. The intertwining of superconductivity and CDW order, however, remains controversial [8,10,11]. Recent observations of a robust CDW order in ultrathin samples [12,13], and discussions on possible chiral nature of the CDW phase [14–17] in bulk $1T$-$TiSe_2$, have further intensified the search for the mechanism of its CDW transition. To this end, identifying subtle details of the electronic and atomic structural features is key to elucidating the CDW phase.

The CDW transition in $1T$-$TiSe_2$ is accompanied by a lattice expansion to a $2 \times 2 \times 2$ superlattice below the transition temperature $T_{CDW} \sim 200$ K [18]. As is the case for a number of other CDW bearing TMDs [19–21], the Fermi surface nesting scenario [22] does not apply to $1T$-$TiSe_2$ either. Existing models of the CDW order can be broadly classified into three categories based on the proposed roles of the lattice and electronic band structures: (i) Involves an excitonic condensation mechanism [23] where excitons are formed above T_{CDW} because of poorly screened Coulomb interactions and the long-range CDW order emerges from Bose-Einstein condensation (BEC) of excitons below T_{CDW}. (ii) Involves a Jahn-Teller (JT)-like distortion mechanism [24,25] where the CDW order is mediated by electron-phonon interactions and the transition occurs through a partial charge transfer between the Se $4p$ valence and Ti $3d$ conduction bands. Two different types of distortions have been proposed in the literature. One is a band type JT-like distortion (BJT) [24] proposed by Hughes, which involves the relative rotation of the top and bottom layers of Se ions in the $1T$-$TiSe_2$ lattice. The other is a pseudo–JT-like distortion (PJT) first put forth by Whangbo and Canadell [25], in which a proposed shortening of the Ti-Se bonds stabilizes the structural distortion below T_{CDW}. And lastly, (iii) incorporates a a hybrid model [26] which is a combination of JT-like distortions and exciton condensation. In this work we explore which of these three scenarios are consistent with our experimental observations.

Earlier ARPES results have been interpreted in the framework of excitonic condensation below T_{CDW} [27,28]. The BEC of excitons below T_{CDW} has also been suggested from momentum-resolved electron energy loss spectroscopy [29]. However, the detection of CDW correlations even after nonthermal melting of the excitonic insulating phase via

*dl4f@virginia.edu
†uc5j@virginia.edu

ultrafast optical spectroscopy [30], is incompatible with a purely electronic origin of the CDW transition. Recent scanning tunneling microscopy (STM) measurements [16] and first-principles calculations [31,32] pointed to the significance of local distortions to the CDW instability in $1T$-$TiSe_2$. These observations call for a direct investigation of the local lattice distortions and of their influence on the electronic structure of $1T$-$TiSe_2$ in the CDW state. Previous measurements have focused on lattice dynamics and mostly looked at the softening of phonon modes [33,34] that were linked to the Di Salvo model, with Ti distortions along the a or b axis. A direct investigation of the local structural distortions, essential to the JT mechanism, is lacking and the focus of the present paper.

In this work we investigated the structural and electronic properties of $1T$-$TiSe_2$ using neutron scattering and ARPES as a function of temperature, complemented by density functional theory (DFT) calculations. Our main results are as follow: (i) Evidence of a breathing-type JT-like local structural distortion is provided from the neutron diffraction data, yielding a splitting of the nearest neighbor Ti-Se bond lengths in the CDW state, that cannot be interpreted in the framework of the Di Salvo model. (ii) Using this local displacement pattern as input in the DFT calculation resulted in a free energy gain that is surprisingly larger compared to that using Di Salvo's displacement pattern. (iii) Lastly, the ARPES measurements provide evidence for a strong temperature dependence of the chemical potential (μ) and a temperature-dependent downward shift of the Se $4p$ valence band, while the Ti $3d$ conduction band remains intact. These results are consistent with the pseudo–JT-like distortion picture as in the theoretical model by Whangbo and Canadell [25].

II. EXPERIMENTAL DETAILS

Temperature-dependent ARPES measurements on $1T$-$TiSe_2$ single crystals were performed using a Scienta R4000 electron analyzer at the PGM beamline of the Synchrotron Radiation Center in Wisconsin and the SIS beamline of the Swiss Light Source, Paul Scherrer Institute, Switzerland. The measurements were performed using plane polarized light with 45 and 56 eV photon energies ($h\nu$). Single crystals were cleaved *in situ* to expose a fresh surface for the ARPES measurements. The neutron diffraction experiments were carried out using the BT-1 diffractometer at the NIST Center for Neutron Research and the Nanoscale Ordered Materials Diffractometer (NOMAD) of Oak Ridge National Laboratory. The data were analyzed both in reciprocal and real space to obtain the average and local structures, respectively. The total structure factor $S(Q)$ obtained from NOMAD was Fourier transformed to provide the pair distribution function $G(r)$ in real space.

III. RESULTS

A. Signatures of the CDW order in ARPES, neutron scattering and electrical transport measurements

The CDW transition is characterized using neutron scattering, electrical resistivity $\rho(T)$ and ARPES. The results are summarized in Fig. 1. Shown in Fig. 1(b) is the temperature dependence of the $\rho(T)$ and its derivative. T_{CDW} is observed at 200 K. At T_{CDW}, a structural transition occurs from the high temperature $P\bar{3}m1$ symmetry to a $2 \times 2 \times 2$ superlattice with a $P\bar{3}c1$ symmetry. Diffraction data collected at BT-1 as a function of temperature are shown in Fig. 1(c). The 7 and 100 K patterns are fit using the $P\bar{3}c1$ low temperature symmetry of Di Salvo. Half-integer reflections such as the $(\frac{1}{2}, 0, 4)$ are observed due to the $2 \times 2 \times 2$ lattice expansion. Above 200 K, the extra reflections due to cell expansion disappear and by 300 K, the structure reverts to the high symmetry $P\bar{3}m1$ phase as reported in the literature. Backfolded energy bands [22] associated with the CDW wave vectors are anticipated in the CDW state [Figs. 1(a) and 1(d)]. Shown in Fig. 1(e) is the crystal structure with the atomic distortions proposed by Di Salvo. Note that the Ti atoms are displaced in the ab plane towards other Ti atoms (indicated with red arrows), and the Se atoms rotate around Ti atoms at (0,0,0) that are not displaced. The Hughes model is based on the Se rotations around the fixed Ti atoms as indicated with the star of David at the upper right corner of the unit cell. CDW backfolded bands are visible in the ARPES energy-momentum intensity maps (EMIMs) shown in Figs. 1(f)–1(i). An EMIM [35] is a representation of the ARPES data as a function of an in-plane momentum component (k_x in the current case) and electronic energy $\overline{\omega}$ referenced to μ. The other orthogonal momentum component (k_y) is kept fixed.

The EMIMs are described in terms of the surface Brillouin zone (BZ) high-symmetry points. The normal emission ARPES spectra with $h\nu = 56$ and 45 eV correspond to the states located in the vicinity of Γ and A points, respectively [Fig. 1(d)]. Therefore, the high symmetry points of Figs. 1(f) and 1(g) are referred by $\overline{\Gamma}$ and $\overline{M}$, while those of Figs. 1(h) and 1(i) by $\overline{A}$ and $\overline{L}$. The energy bands closest to μ around $\overline{\Gamma}$ and $\overline{A}$ are due to the Se $4p$ bands, while those around $\overline{M}$ and $\overline{L}$ correspond to the Ti $3d$ bands. The formation of a $2 \times 2 \times 2$ CDW order leads to backfolding of the Se $4p$ bands at $\overline{L}$ and $\overline{M}$ points below T_{CDW}. This can be observed from Figs. 1(g) and 1(i), which correspond to a temperature $\sim 40\,\mathrm{K} < T_{CDW}$. Moreover, the backfolded bands are practically nonexistent in Figs. 1(f) and 1(h), which correspond to a temperature $\sim 285\,\mathrm{K} > T_{CDW}$. Some residual intensity from the backfolded bands is, however, visible even above T_{CDW} as seen in Figs. 1(f) and 1(h). This is probably due to short-range CDW correlations above T_{CDW}. These results are in agreement with previous ARPES studies on this system [10,11,27,28,36,37].

B. Pair correlation function in the CDW state

To carefully examine the structure in the CDW phase, we turn our attention to the pair correlation function. The $G(r)$ of Fig. 2 corresponds to the local atomic structure at 2 K obtained from the Fourier transform of the diffraction data collected on NOMAD. The experimentally obtained $G(r)$ is compared to a model $G(r)$ calculated using the atomic coordinates and unit cell dimensions based on the Di Salvo model [18]. The first negative peak in $G(r)$ corresponds to the Ti-Se bonds while the second peak corresponds to Ti-Ti and Se-Se bonds. Note that the first peak is negative because Ti has a negative neutron scattering length [38]. In the Di Salvo

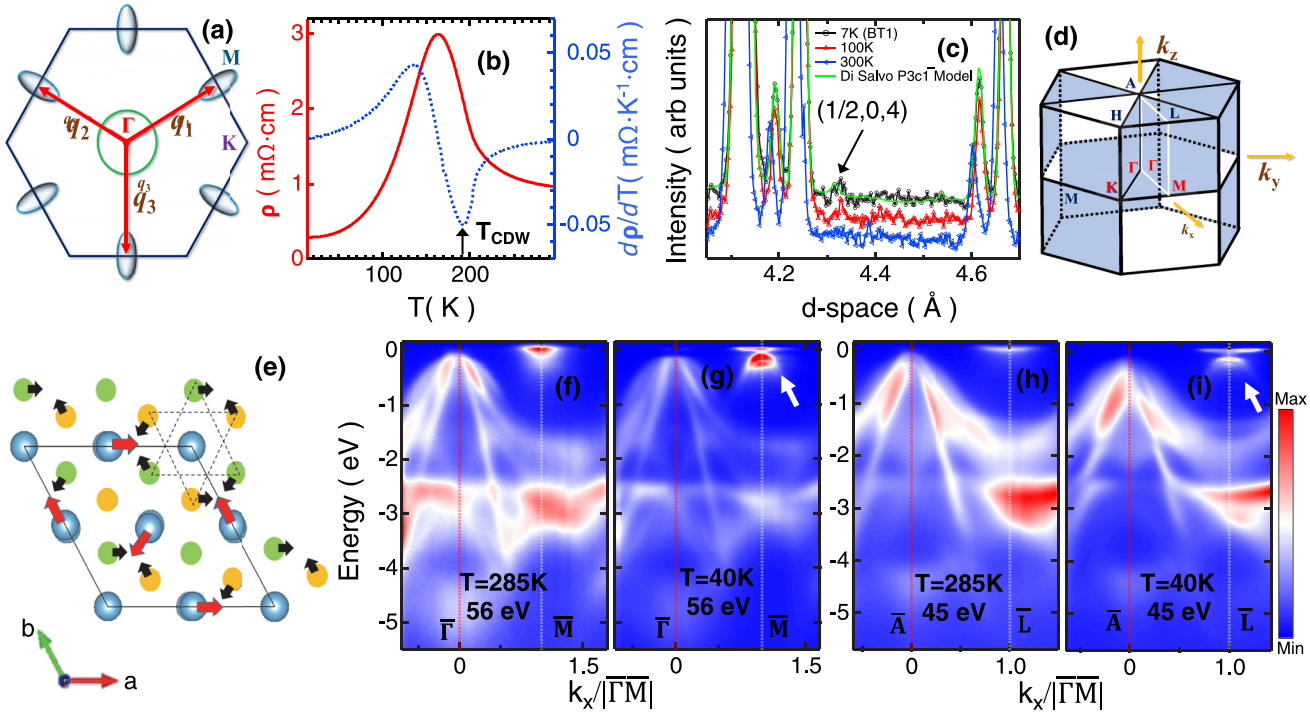

FIG. 1. (a) Schematic plot illustrates connections among various sections of the Fermi surfaces via CDW wave vectors $\mathbf{q_1}$, $\mathbf{q_2}$, and $\mathbf{q_3}$. (b) Temperature (T) dependence of ρ (red solid curve) of $1T$-$TiSe_2$. T_{CDW} is determined from the minimum (pointed by the black arrow) of $\frac{d\rho}{dT}$ vs T plot (black dashed line). (c) The (1/2, 0, 4) Bragg peak in the neutron scattering data corresponds to the CDW superlattice. Its intensity below T_{CDW} diminishes with increasing temperature and it vanishes above T_{CDW}. (d) Schematic layout of the normal state Brillouin zone of $1T$-$TiSe_2$. (e) The Di Salvo crystal structure model for the CDW phase of $1T$-$TiSe_2$. (f) and (g) EMIMs with $h\nu = 56$ eV at $T = 285$ K and $T = 40$ K, respectively. (h) and (i) Same as (f) and (g) but with $h\nu = 45$ eV. The red dotted lines correspond to $\overline{\Gamma}$ in (f) and (g), while to $\overline{A}$ in (h) and (i). The white dotted lines refer to $\overline{M}$ in (f) and (g), while to $\overline{L}$ in (h) and (i). The white arrows in (g) and (i) indicate the backfolding of Se $4p$ bands below T_{CDW} at $\overline{M}$ and $\overline{L}$, respectively.

model, the Ti atoms are displaced towards other Ti atoms and the magnitude of the displacement is 0.085 Å, as shown in Fig. 1(a), while displacement of the Se atoms toward other Se atoms is 0.028 Å. These distortions give rise to a broad Ti-Se peak with a full-width-half maximum of 0.13 Å. While the overall fitting is good with a $\chi^2 \sim 0.592$, this model fails to reproduce the splitting of the first Ti-Se bond pairs at 2.55 Å seen as a shoulder to the left of the first peak [see Fig. 2(a)]. Shown in Fig. 2(b) is a comparison of the same 2 K data plotted in Fig. 2(a) with a new model $G(r)$ that is calculated based on a local model that reproduces the split of the Ti-Se correlations well [see inset of Fig. 2(b)]. Using the local model, it can be seen that the split of the Ti-Se correlation peak to long and short bonds can be fit by two Gaussian curves centered at ~2.39 and 2.55 Å. For comparison, in the Di Salvo model, the Ti-Se nearest neighbor bond lengths range from 2.50 to 2.57 Å. Thus the change in the bond lengths expected in the Di Salvo model is not sufficiently large to explain the 0.16 Å peak split observed in the data at 2 K.

The split of the Ti-Se bonds indicates the presence of a JT-like distortion, and is consistent with the proposal put forward by Whangbo and Canadell. To reproduce the split of the Ti-Se pair correlation peak, the symmetry is lowered from the $P\bar{3}c1$ symmetry used by Di Salvo which only allows the Ti atoms to move toward other Ti atoms. The local model that best fits the Ti-Se distortions observed in the data is constructed using the high temperature $P\bar{3}m1$ symmetry that allows refinement of the Ti and Se atomic coordinates. A $2 \times 2 \times 2$ lattice modulation and $a = b = 7.05232 \pm 0.00008$ Å and $c = 11.9816 \pm 0.0003$ Å was set. This model especially fits the Ti-Se pair correlations as seen in Fig. 2(b) and in the inset, and the agreement is quite good overall. The χ^2 of this fit is 0.252.The magnitude of the atom displacements does not deviate much from the Di Salvo model but the direction changes and the details of the Ti and Se motions is shown in Fig. 2(c). The resulting local model involves trigonal distortions of Ti towards Se atoms above and below the Ti plane as shown in Fig. 2(c). There are no in-plane Se rotation around Ti atoms. To further check the validity of this model, the diffraction data shown in Fig. 1(c) at 7 K from BT-1 is fit using the atomic coordinates obtained from the local model, and the comparison in shown in Fig. 2(d). The fitting is as good as in Fig. 1(c). Both models are successful in predicting the position of the ($\frac{1}{2}$, 0, 4) peak. Both models have the same lattice parameters, and index the same peaks. Both models reproduce the diffraction data well, suggesting that the average structure can be fit by both models equally well. But when fitting the local structure is concerned, the Di Salvo model does not work well because of the pseudo–JT splitting. The JT splitting can only come about with the Ti distortions shown in Fig. 2(c). Furthermore, we observe that this local distortion model results in a larger

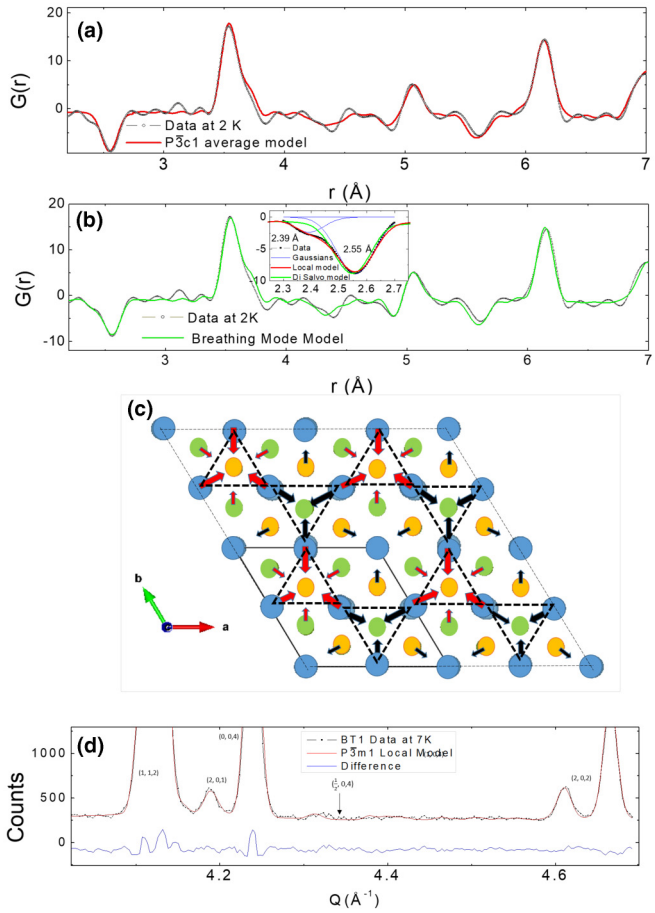

FIG. 2. (a) The $G(r)$ is compared to the model proposed by Di Salvo [18]. This model does not reproduce the splitting of the first nearest Ti-Se bonds. (b) The $G(r)$ is compared to a local model shown in (c) that reproduces the splitting of the first peak. A close up of the first peak is shown in the inset. It is compared to the local model and the Di Salvo model. (c) An expanded view of four superlattice unit cells showing the breathing mode motif, indicated by arrows. (d) The neutron diffraction data at 7 K is compared to the local model shown of (c). The superlattice peak associated with the CDW is reproduced.

energy gain in comparison with the distortion proposed by Di Salvo from our DFT calculations (see the Supplemental Material [39]). This indicates that the proposed breathing-type distortion can be a viable option for the CDW state in $1T$-$TiSe_2$.

We next discuss the implications of our structural data in the context of BJT and PJT scenarios. For BJT-like distortions proposed by Hughes [24], the Se atom rotations do not yield a split Ti-Se peak and is thus inconsistent with the local structure data. The PJT-like distortions in the model of Whangbo and Canadell, however, can naturally give rise to shortening and lengthening of bond lengths. This agrees with our local model, although the magnitude of the distortion was not given in their theoretical model. The large splitting of the Ti-Se peak observed in the $G(r)$ most likely arises from a JT-like mechanism. This Ti-Se bond shortening is crucial to the stabilization of the lattice distortion of $1T$-$TiSe_2$ below T_{CDW}, which was also conjectured in a recent STM work [16].

C. DFT analysis

The DFT calculations (see the Supplemental Material [39]) using the Di Salvo's model as well as the locally distorted model determined in this study were performed with the VASP [40] package using the SCAN-rvv10 [41] exchange-correlation potential for accurate modeling of van der Waals interactions. The details of the calculation and the resulting band structures are provided in the Supplemental Material. Overall, the electronic bands, observed from our DFT calculations agree well with previous results. The highlight of our calculations, however, is the finding that our proposed "breathing mode" structure has a slightly lower energy than the structure proposed by Di Salvo. Therefore, it should be considered as a plausible candidate for the displacement pattern in the CDW state of $1T$-$TiSe_2$.

D. Temperature dependence of the chemical potential and valence bands

In both the BJT and PJT models [24,25], exchange of single-particle spectral weights between the Se $4p$ valence and Ti $3d$ conduction bands are responsible for the net reduction in the free energy of the CDW state over the normal state. With decreasing temperature through T_{CDW}, the energy lowering for the BJT and PJT models occurs via a downward movement of the Ti $3d$ and Se $4p$ bands, respectively. In order to distinguish between these two scenarios, it is necessary to compare the temperature-dependent changes in the valence and conduction bands. To do so, the effects of the Fermi function (FF) and the energy resolution are to be eliminated from the ARPES data. This can be accomplished to a good approximation by dividing the ARPES data with the resolution broadened FF [42]. The temperature-dependent shifts of the valence and conduction bands can be quantified by tracking the temperature-dependent changes in the FF-divided energy distribution curves (EDCs) at $\overline{\Gamma}$ and $\overline{M}$ points, respectively. In this context, an EDC is the ARPES data as a function of $\overline{\omega}$ at a specific momentum value. As can be realized from Figs. 3(c) and 3(d), the peaks of the FF-divided EDCs both at the $\overline{\Gamma}$ and $\overline{M}$ shift towards $\overline{\omega} = 0$ with increasing temperature. In other words, both the valence and conduction bands seem to move towards a higher binding energy as the temperature is decreased from 280 ($> T_{CDW}$) to 70 K ($< T_{CDW}$). The magnitude of the shift of the valence band is, however, substantially larger than that of the conduction band. From these changes, the PJT and BJT scenarios cannot be differentiated from the ARPES data, unless the temperature dependence of $\mu(T)$ is taken into account. The shift in μ of a material results in a global shift of its electronic bands. One way to approximate this is to explore the rigid shift of some feature of the valence band, located sufficiently far away from μ [42]. This has been shown in Fig. 3(f) by comparing valence band features that correspond to the momentum marked by the black dashed line in Fig. 1(f), at $T = 70$ and 280 K. A global shift of the bands can also be approximated from a shift in core level peaks [42–47]. We determined this by monitoring the Se $3d_{3/2}$ and $3d_{5/2}$ core level peaks at $T = 70$ and 280 K in Fig. 3(e). The magnitude of the shift in μ obtained from Fig. 3(e) is consistent with that from Fig. 3(f). Given that $1T$-$TiSe_2$ is either a semimetal or a semiconductor with a very

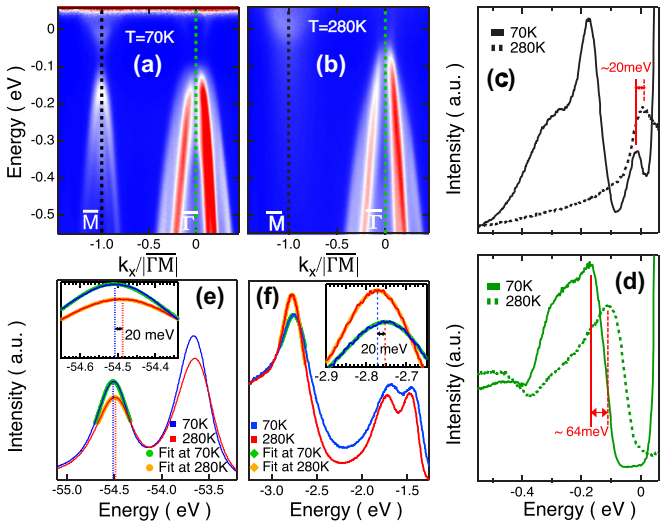

FIG. 3. The EMIMs after being divided by the resolution-broadened Fermi function at (a) 70 K and (b) 280 K. Both data were collected with $h\nu = 56$ eV. The green and black dotted lines correspond to $\overline{\Gamma}$ and $\overline{M}$ in (a) and (b), respectively. (c) Fermi function-divided EDCs at the $\overline{M}$ point for $T \sim 70$ and 280 K. (d) Same as (c) but at the $\overline{\Gamma}$ point. (e) Core level spectra of Se with a focus on the Se $3d_{3/2}$ and $3d_{5/2}$ peaks at $T = 70$ and 280 K. Inset shows an expanded view of the Se $3d_{3/2}$ peaks at 70 and 280 K. (f) Valence band spectra associated with the momentum location, denoted by the black dotted line in Fig. 1(f), at energies sufficiently away from μ for $T = 40$ and 280 K.

small band gap, a temperature-dependent μ is not unexpected. We observed that the shift in μ is practically the same as the drift of the conduction band in Fig. 3(c) within experimental error. Therefore, the temperature-dependent change of the band minima of the Ti $3d$ conduction bands is rooted to $\mu(T)$, while the evolution of the maxima of the Se $4p$ valence band with temperature is indeed nontrivial.

IV. CONCLUSIONS

To summarize, an experimental observation of JT-like local breathing-type distortions in the CDW state of $1T$-$TiSe_2$ is reported. DFT calculations based on the local model result in an energy gain that is larger in comparison to that obtained considering the Di Salvo model of the CDW. This indicates that the proposed displacement pattern is a possible candidate for the structural distortion in the CDW state of $1T$-$TiSe_2$. From the ARPES data it is shown that by factoring out the temperature dependence of μ, it is the valence band that shifts towards a higher binding energy while the conduction band remains intact. These observations are indicative of the pseudo–JT-like distortion picture of the CDW instability of $1T$-$TiSe_2$ as proposed in the theoretical model of Whangbo and Canadell [25].

ACKNOWLEDGMENTS

U.C. acknowledges supports from the National Science Foundation (NSF) under Grant No. DMR-1629237 and from the Jefferson Trust at the University of Virginia. D.L. acknowledges support from the U.S. Department of Energy, contract No. DE-FG02-01ER45927. G.K. and A.A.A. acknowledges support from the NSF under Grant No. ECCS-1711015. U.C. thankfully acknowledges fruitful discussions with J. van Wezel. A portion of this research used resources at the Spallation Neutron Source, a DOE Office of Science User Facility operated by the Oak Ridge National Laboratory. We acknowledge the support of the National Institute of Standards and Technology, U.S. Department of Commerce, in providing the neutron research facilities used in this work.

[1] J. G. Bednorz and K. A. Müller, Z. Phys. **64**, 189 (1986).
[2] G. R. Stewart, Rev. Mod. Phys. **83**, 1589 (2011).
[3] E. Dagotto, New J. Phys. **7**, 67 (2005).
[4] Edited by T. Kasuya and T. Saso, *Theory of Heavy Fermions and Valence Fluctuations, Proceedings of the Eighth Taniguchi Symposium* (Springer-Verlag, Berlin, Heidelberg, 1985).
[5] J. A. Wilson and A. D. Yoffe, Adv. Phys. **18**, 193 (1969).
[6] K. Rossnagel, J. Phys.: Condens. Matter **23**, 213001 (2011).
[7] L. J. Li, E. C. T. O. Farrell, K. P. Loh, G. Eda, B. Ozyilmaz and A. H. Castro Neto, Nature (London) **529**, 185 (2016).
[8] E. Morosan, H. W. Zandbergen, B. S. Dennis, J. W. G. Bos, Y. Onose, T. Klimczuk, A. P. Ramirez, N. P. Ong, and R. J. Cava, Nat. Phys. **2**, 544 (2006).
[9] A. F. Kusmartseva, B. Sipos, H. Berger, L. Forró, and E. Tutiš, Phys. Rev. Lett. **103**, 236401 (2009).
[10] J. F. Zhao, H. W. Ou, G. Wu, B. P. Xie, Y. Zhang, D. W. Shen, J. Wei, L. X. Yang, J. K. Dong, M. Arita, H. Namatame, M. Taniguchi, X. H. Chen, and D. L. Feng, Phys. Rev. Lett. **99**, 146401 (2007).
[11] D. Qian, D. Hsieh, L. Wray, E. Morosan, N. L. Wang, Y. Xia, R. J. Cava, and M. Z. Hasan, Phys. Rev. Lett. **98**, 117007 (2007).
[12] P. Chen, Y.-H. Chan, X.-Y. Fang, Y. Zhang, M. Y. Chou, S.-K. Mo, Z. Hussain, A.-V. Fedorov, and T.-C. Chiang, Nat. Commun. **6**, 8943 (2015).
[13] K. Sugawara, Y. Nakata, R. Shimizu, P. Han, T. Hitosugi, T. Sato, and T. Takahashi, ACS Nano. **10**, 1341 (2016).
[14] J.-P. Castellan, S. Rosenkranz, R. Osborn, Q. Li, K. E. Gray, X. Luo, U. Welp, G. Karapetrov, J. P. C. Ruff, and J. van Wezel, Phys. Rev. Lett. **110**, 196404 (2013).
[15] J. Ishioka, Y. H. Liu, K. Shimatake, T. Kurosawa, K. Ichimura, Y. Toda, M. Oda, and S. Tanda, Phys. Rev. Lett. **105**, 176401 (2010).
[16] B. Hildebrand, T. Jaouen, C. Didiot, E. Razzoli, G. Monney, M.-L. Mottas, F. Vanini, C. Barreteau, A. Ubaldini, E. Giannini, H. Berger, D. R. Bowler, and P. Aebi, Phys. Rev. B **95**, 081104(R) (2017).
[17] B. Hildebrand, T. Jaouen, M.-L. Mottas, G. Monney, C. Barreteau, E. Giannini, D. R. Bowler, and P. Aebi, Phys. Rev. Lett. **120**, 136404 (2018).

[18] F. Di Salvo, D. Moncton, and J. Waszczak, Phys. Rev. B **14**, 4321 (1976).
[19] U. Chatterjee, J. Zhao, M. Iavarone, R. Di Capua, J. P. Castellan, G. Karapetrov, C. D. Malliakas, M. G. Kanatzidis, H. Claus, J. P. C. Ruff, F. Weber, J. van Wezel, J. C. Campuzano, R. Osborn, M. Randeria, N. Trivedi, M. R. Norman, and S. Rosenkranz, Nat. Commun. **6**, 6313 (2015).
[20] J. Zhao, K. Wijayaratne, A. Butler, J. Yang, C. D. Malliakas, D. Y. Chung, D. Louca, M. G. Kanatzidis, J. van Wezel, and U. Chatterjee, Phys. Rev. B **96**, 125103 (2017).
[21] K. Wijayaratne, J. Zhao, C. Malliakas, D. Y. Chung, M. G. Kanatzidis, and U. Chatterjee, J. Mater. Chem. C **5**, 11310 (2017).
[22] G. Grüner, Rev. Mod. Phys. **60**, 1129 (1988).
[23] L. V. Keldysh and Y. V. Kopaev, Sov. Phys. Solid State **6**, 2219 (1965).
[24] H. Hughes, J. Phys. C **10**, L319 (1977).
[25] M. Whangbo and E. Canadell, J. Am. Chem. Soc. **114**, 9587 (1992).
[26] J. van Wezel, P. Nahai-Williamson, and S. S. Saxena, Europhys. Lett. **89**, 47004 (2010).
[27] H. Cercellier, C. Monney, F. Clerc, C. Battaglia, L. Despont, M. G. Garnier, H. Beck, P. Aebi, L. Patthey, H. Berger, and L. Forró, Phys. Rev. Lett. **99**, 146403 (2007).
[28] C. Monney, H. Cercellier, F. Clerc, C. Battaglia, E. F. Schwier, C. Didiot, M. G. Garnier, H. Beck, P. Aebi, H. Berger, L. Forró, and L. Patthey, Phys. Rev. B **79**, 045116 (2009).
[29] A. Kogar, M. S. Rak, S. Vig, A. A. Husain, F. Flicker, Y. Il Joe, L. Venema, G. J. MacDougall, T. C. Chiang, E. Fradkin, J. van Wezel, and P. Abbamonte, Science **358**, 1314 (2017).
[30] M. Porer, U. Leierseder, J.-M. Ménard, H. Dachraoui, L. Mouchliadis, I. E. Perakis, U. Heinzmann, J. Demsar, K. Rossnagel, and R. Huber, Nat. Mater. **13**, 857 (2014).
[31] H. Watanabe, K. Seki, and S. Yunoki, Phys. Rev. B **91**, 205135 (2015).
[32] M. Calandra and F. Mauri, Phys. Rev. Lett. **106**, 196406 (2011).
[33] M. Holt, P. Zschack, Ha. Hong, M. Y. Chou, and T.-C. Chiang, Phys. Rev. Lett. **86**, 3799 (2001).
[34] F. Weber, S. Rosenkranz, J.-P. Castellan, R. Osborn, G. Karapetrov, R. Hott, R. Heid, K.-P. Bohnen, and A. Alatas, Phys. Rev. Lett. **107**, 266401 (2011).
[35] J. Zhao, C. D. Malliakas, K. Wijayaratne, V. Karlapati, N. Appathurai, D. Y. Chung, S. Rosenkranz, M. G. Kanatzidis, and U. Chatterjee, Europhys. Lett. **117**, 27006 (2017).
[36] Th. Pillo, J. Hayoz, H. Berger and F. Lévy, L. Schlapbach, and P. Aebi, Phys. Rev. B **61**, 16213 (2000).
[37] K. Rossnagel, L. Kipp, and M. Skibowski, Phys. Rev. B **65**, 235101 (2002).
[38] V. F. Sears, Neutron News **3**, 26 (1992).
[39] See Supplemental Material at http://link.aps.org/supplemental/10.1103/PhysRevB.101.195145 for the atomic coordinates, multiplicities, and Wyckoff letter of the atoms in the high temperature phase of 1T-$TiSe_2$ incorporated in the calculations of $G(r)$ using various models; and for band structures with local displacement and Di Salvo's displacement pattern as input in the DFT calculations.
[40] G. Kresse, and J. Furthmüller, Phys. Rev. B **54**, 11169 (1996); Comput. Mater. Sci **6**, 15 (1996).
[41] H. Peng, Z. H. Yang, J. P. Perdew, and J. Sun, Phys. Rev. X **6**, 041005 (2016).
[42] S. Hüfner, *Photoelectron Spectroscopy* (Springer, Berlin, 2003).
[43] K. Ebata, H. Wadati, M. Takizawa, A. Fujimori, A. Chikamatsu, H. Kumigashira, M. Oshima, Y. Tomioka, and Y. Tokura, Phys. Rev. B **74**, 064419 (2006).
[44] P. Pal, P. Kumar, Aswin V., A. Dogra, and A. G. Joshi, J. Appl. Phys. **116**, 053704 (2014).
[45] J. Matsuno, A. Fujimori, Y. Takeda, and M. Takano, Europhys. Lett. **59**, 252 (2002).
[46] A. Fujimori, A. Ino, J. Matsuno, T. Yoshida, K. Tanaka, T. Mizokawa, J. Electron Spectrosc. Relat. Phenom. **124**, 127 (2002).
[47] K. M. Shen, F. Ronning, D. H. Lu, W. S. Lee, N. J. C. Ingle, W. Meevasana, F. Baumberger, A. Damascelli, N. P. Armitage, L. L. Miller, Y. Kohsaka, M. Azuma, M. Takano, H. Takagi, and Z.-X. Shen, Phys. Rev. Lett. **93**, 267002 (2004).